Analytical solutions for the isobaric evaporation of pure cryogens in storage tanks

Felipe Huerta and Velisa Vesovic*

Department of Earth Science and Engineering, Imperial College London,

London SW7 2AZ, United Kingdom

*corresponding author: Tel: +44 20 7594 7352, E-mail: v.vesovic@imperial.ac.uk

Abstract

New analytical solutions have been derived for the isobaric evaporation of a pure liquid cryogen. In particular, expressions have been provided for the liquid volume, evaporation rate, Boil-off-Gas (BOG) rate, vapour temperature and vapour to liquid heat transfer rate as a function of time. Both equilibrium and non-equilibrium scenarios have been considered. In the former, the vapour and liquid cryogen are assumed to be in thermal equilibrium, while in the latter the vapour is treated as superheated with respect to the liquid and acts as an additional heat source.

The derived solutions for two scenarios were validated against the numerical results for the evaporation of liquid methane and of liquid nitrogen in small, medium sized and large storage tanks that are used in industry. For the equilibrium model, the analytical solutions are exact. For the non-equilibrium model, the analytical solutions are valid for the whole duration of evaporation, except for a short transient period at the beginning of the evaporation. For physical quantities of industrial interest, they provide accurate estimates of liquid volume, BOG rate and BOG temperature, with the maximum deviations not exceeding 1%, 2% and 4.5%, respectively. The vapour to liquid heat transfer rate is also well predicted to within a maximum deviation of 5%.

Keywords: cryogen, LNG, weathering, boil-off gas

1. Introduction

Cryogenic liquids are widely used in industry in a number of operations, primarily in refrigeration [1], power generation [2] and as rocket fuel [3]. Recently, the usage of cryogenic liquids has been extended to novel applications such as hydrogen production [4], energy storage [5, 6] and carbon dioxide capture by cryogenic separation [7-9]. Cryogenic liquids are traditionally classified as substances with a normal boiling point below -150°C, and as such are stored in highly insulated vessels, which are nevertheless subject to heat ingress driven by the large temperature gradient between the surroundings and stored cryogen. The heat intrusion drives a number of complex transport phenomena within a cryogen, including natural convection, evaporation/condensation, thermal stratification and liquid thermal expansion; thus raising engineering, safety, economic and environmental challenges.

One of the major cryogenic storage applications is the storage of liquefied natural gas (LNG) in large tanks at constant operating pressure, slightly above the atmospheric. In LNG storage, the heat ingress evaporates the LNG, and the vapour is continuously removed from the tank to keep the tank pressure constant. The vapour which leaves the tank is denominated boil-off gas (BOG), and its continuous removal produces weathering, as methane and nitrogen preferentially evaporate. The resulting changes in thermophysical properties of the remaining LNG may limit its marketability and may produce safety hazards such as rollover [10].

The storage of liquid hydrogen (LH_2), in small to mid-sized vessels at variable pressure up to 1 MPa, is another example. In this application, the cryogenic liquid is extremely valuable, and discarding the evaporated hydrogen from the tank is neither economical nor safe. Without BOG removal, the evaporation is non-isobaric, and a complex coupling is present between self-pressurization, evaporation/condensation and thermal stratification in both vapour and liquid phases [3, 11]. Minimizing the evaporation of LH_2 stored in tanks in space vehicles influences the planning and execution of space explorations mission [12], and increases the driving range in hydrogen-powered vehicles [13]. However, not all storage of liquid hydrogen is carried out under non-isobaric conditions. The isobaric evaporation of LH_2 is present in the

storage tanks with vapour cooling shields (VCS), where the evaporated hydrogen is constantly removed as BOG and used to improve the insulation efficiency [14].

Isobaric storage is more frequent for cheaper cryogens, such as liquid nitrogen (LN_2). LN_2 storage tanks have capacities between 2 and 100 m^3 [15], operate at a constant pressure, and can be found typically in bulk delivery systems or as buffer vessels in LN_2 energy storage systems [16]. Predicting BOG rates and vapour temperatures is relevant in both applications. In the former, it helps in achieving more optimal design of the process equipment, while in energy storage systems, it allows for a better prediction of the turnover efficiency of the power cycle during the discharge.

For both isobaric and non-isobaric evaporation of cryogenic liquids, experimental data is scarce and most research work has been focused on developing phenomenological models. Although a plethora of models does exist [11, 17-32] the validation still remains a major issue, due in part to a lack of reliable data. The models themselves exhibit a number of areas of disagreement, where further work is necessary, especially in describing the vapour phase evolution. For instance, a recent review [33] highlighted major discrepancies in the prediction of the vapour temperature profiles and vapour to liquid heat transfer between a number of non-isobaric CFD evaporation models. In the isobaric evaporation of cryogens, the transport phenomena are significantly simpler as the liquid temperature can be assumed thermally homogeneous and there is no self-pressurization. Most work on the evaporation of cryogens under isobaric or nearly isobaric conditions focuses on modelling of LNG weathering. Early models have assumed that both vapour and liquid cryogen are in thermal equilibrium [17, 20, 21, 23, 24, 26, 34-40], while the most recent weathering models [25, 32, 41-44], have incorporated a non-equilibrium approach, based on experimental and industrial data; thus, the vapour is treated as superheated with respect to the liquid and acts as an additional heat source.

The objective of this work is to derive analytical solutions for isobaric evaporation of pure cryogens stored in closed tanks. In this context, the term closed tank refers to a standard storage tank used in industry that is not open to the atmosphere and where the pressure is regulated by means of a pressure relief valve. The derived solutions will

provide an easy to use tool for practitioners to estimate the liquid volumes, evaporation rates, BOG rates, BOG temperatures and vapour temperature profiles during the cryogen storage and hence improve the BOG management processes. The solutions can also act as limiting case scenarios that can be used to test different models. From a scientific point of view, they provide for a clearer insight into the driving forces that govern evaporation and help in easily ascertaining how sensitive calculated values are to particular parameters; something that with more complicated models and especially CFD models is not always apparent.

In section 2 we derive analytical solutions based on the non-equilibrium weathering model of Huerta and Vesovic [43]. In section 3 we validate the developed analytical solutions, by comparing to the numerical results for the evaporation of liquid methane and nitrogen, and provide the range of their validity. A summary and conclusions of the results are given in section 4.

2. Analytical Solutions

2.1 Weathering Model

In order to provide analytical solutions for the evaporation of a pure cryogen, in a cylindrical storage tank under constant pressure, we take Huerta and Vesovic model of LNG weathering [43] as the starting point. Only the relevant features of the weathering model are summarized in this work, and the interested reader is referred to the original work for the full description.

Figure 1 summarizes the main heat and mass transfer processes that occur during the isobaric storage of cryogen in cylindrical tanks. Three different heat flows from the surroundings are depicted: through the tank roof, $\dot{Q}_{\mathrm{roof}}$, through the bottom of the tank, $\dot{Q}_{\mathrm{bot}}$, and through the wall. The heat ingress through the wall is divided into the heat transfer rate to the liquid, $\dot{Q}_{\mathrm{L}}$, and to the vapour, $\dot{Q}_{\mathrm{V}}$. Inside the tank, the liquid and vapour phases are assumed separated by a smooth interface. If the vapour, as a result of heating, attains higher temperature than liquid, it can act as an additional heat source, in which case there is a further heat flow into the liquid, depicted by a vapour to liquid heat transfer rate $\dot{Q}_{\mathrm{VL}}$.

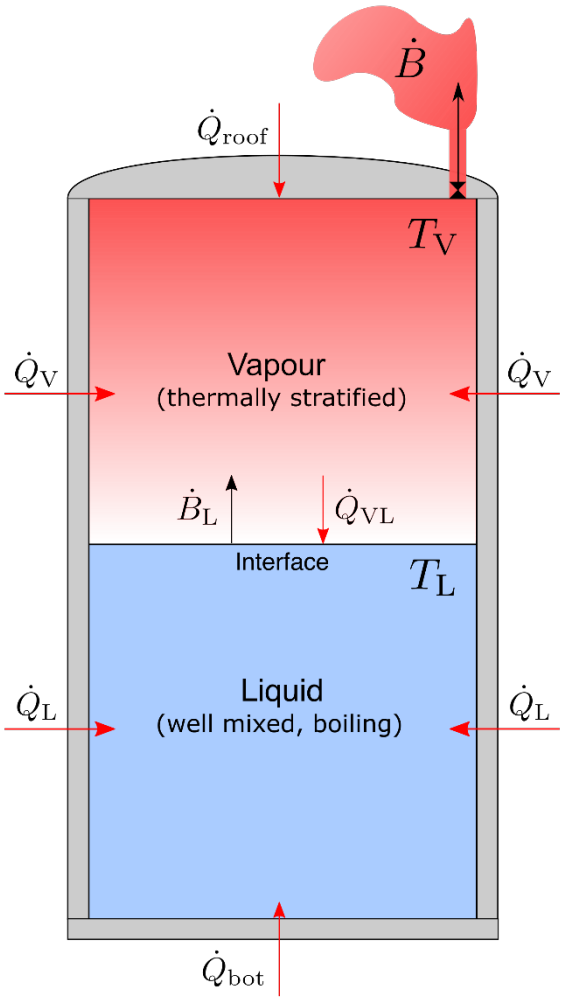

Figure 1: Schematic of the modelled cryogenic storage tank where the vapour and the liquid subsystems were assumed separated by a smooth, horizontal surface. The red and black arrows represent heat and mass flows, respectively.

We assume that the cryogen is stored at its saturation temperature, T_{L}, at a given constant operating pressure P. The heat transfer into the liquid will lead to evaporation at an evaporation rate $\dot{B}_{\mathrm{L}}$. The vaporized cryogen flows upwards and is heated in the vapour space. To keep the tank pressure constant, most of the vapour is removed from the storage tank as boil-off gas (BOG) at a rate $\dot{B}$. The evaporation rate $\dot{B}_{\mathrm{L}}$ and the BOG rate $\dot{B}$ can be evaluated by performing mass balances in the liquid subsystem and in the storage tank,

$$-\dot{B}_{\mathrm{L}} = \frac{d}{dt}(\rho_{\mathrm{L}} V_{\mathrm{L}}) \,, \tag{1}$$

$$-\dot{B} = \frac{d}{dt}(\rho_{\mathrm{L}} V_{\mathrm{L}} + \bar{\rho}_{\mathrm{V}} V_{\mathrm{V}}) = -\dot{B}_{\mathrm{L}} + \frac{d}{dt}(\bar{\rho}_{\mathrm{V}} V_{\mathrm{V}}) \,, \tag{2}$$

where ρ is the density, V is the volume, and the subscripts L and V indicate the liquid and vapour phases, respectively. The average vapour density, $\bar{\rho}_{\mathrm{V}}$, is defined as the vapour density evaluated at the average vapour temperature. The rate of change of liquid volume can be obtained by performing an energy balance over the liquid,

$$\frac{dV_{\mathrm{L}}}{dt} = -\frac{1}{\rho_{\mathrm{L}}}\left(\frac{\dot{Q}_{\mathrm{L,tot}} - \rho_{\mathrm{L}} V_{\mathrm{L}} \frac{dh_{\mathrm{L}}}{dt}}{h_{\mathrm{V}}(T_{\mathrm{L}}) - h_{\mathrm{L}}(T_{\mathrm{L}})} + V_{\mathrm{L}} \frac{d\rho_{\mathrm{L}}}{dt}\right), \tag{3}$$

where h is the enthalpy and $\dot{Q}_{\mathrm{L,tot}}$ is the total liquid heat ingress defined by,

$$\dot{Q}_{\mathrm{L,tot}} = \dot{Q}_{\mathrm{L}} + \dot{Q}_{\mathrm{bot}} + \dot{Q}_{\mathrm{VL}} \,. \tag{4}$$

As the volume of the tank is fixed, the decrease in the volume of one phase must be equal to the increase in the volume of the other phase, $dV_{\mathrm{L}}/dt = -dV_{\mathrm{V}}/dt$.

The heat ingress through the walls occurs by mixed natural convection and conduction and, assuming no heat accumulation in the tank wall, is given by,

$$\dot{Q}_i = U_i A_i (T_{\mathrm{air}} - T_i), \qquad i = \mathrm{L\ or\ V} \tag{5}$$

where U is the overall heat transfer coefficient based on the external area, T_{air} the air temperature and A is the area of the external tank wall. The cylindrical tank has an internal diameter d_{i}, an external diameter d_{o}, a height l and a total volume V_{T}. For this geometry, the liquid and vapour heat ingress areas are linear functions of the liquid volume: $A_{\mathrm{L}} = 4V_{\mathrm{L}}\, d_{\mathrm{o}}/d_{\mathrm{i}}^2$, $A_{\mathrm{V}} = 4(V_{\mathrm{T}} - V_{\mathrm{L}})\, d_{\mathrm{o}}/d_{\mathrm{i}}^2$. If the bottom of the tank is heated to prevent ground freezing, the heat transfer rate $\dot{Q}_{\mathrm{bot}}$ is a model input, whereas if it suspended above an insulation layer, it can be calculated from an equation analogous to Eq. (5).

The vapour to liquid heat transfer rate is assumed to be by conduction [43] and is given by,

$$\dot{Q}_{\mathrm{VL}} = \frac{\pi d_{\mathrm{i}}^2}{4} k_{\mathrm{V}}|_{z=0} \left.\frac{\partial T_{\mathrm{V}}}{\partial z}\right|_{z=0}, \tag{6}$$

where z is the vertical coordinate in the vapour subsystem, $k_{\mathrm{V}}|_{z=0}$ is the vapour thermal conductivity evaluated at the interface temperature and T_{V} is the vapour temperature.

The vapour temperature profile is required to calculate the temperature gradient at the vapour liquid interface. The weathering model [43] assumes that the heat ingress through the wall in the vapour generates a buoyancy driven flow in a thin boundary layer adjacent to the tank wall. The warmer vapour flows upwards through this layer, and then mixes efficiently in the radial direction in the top of the tank. Hence, the temperature vapour domain is defined as the one-dimensional domain $\Omega{:}\,[0, l_{\mathrm{V}}(t)]$ where 0 represents the vapour liquid interface and $l_{\mathrm{V}}(t)$ the height of the vapour phase. The transient vapour temperature profile is governed by the one-dimensional advection-diffusion equation with wall heating as a source term [43],

$$\frac{\partial T_{\mathrm{V}}}{\partial t} = \bar{\alpha}_{\mathrm{V}} \frac{\partial^2 T_{\mathrm{V}}}{\partial z^2} - \frac{4\dot{B}_{\mathrm{L}}}{\bar{\rho}_{\mathrm{V}} \pi d_{\mathrm{i}}^2} \frac{\partial T_{\mathrm{V}}}{\partial z} + \frac{\bar{\alpha}_{\mathrm{V}}}{\bar{k}_{\mathrm{V}}} \frac{4 U_{\mathrm{V}} d_{\mathrm{o}}}{d_{\mathrm{i}}^2} (T_{\mathrm{air}} - T_{\mathrm{V}}) , \tag{7}$$

subject to the following boundary conditions,

$$T_{\mathrm{V}}(z) = T_{\mathrm{L}} , \;\; t = 0,$$

$$T_{\mathrm{V}}|_{z=0} = T_{\mathrm{L}}(t) ,$$

$$\left.\frac{\partial T_{\mathrm{V}}}{\partial z}\right|_{z=l_V} = \frac{\dot{Q}_{\mathrm{roof}}}{k_{\mathrm{V}}|_{z=l_{\mathrm{V}}} A_{\mathrm{roof}}} . \tag{8}$$

where $\bar{\alpha}_{\mathrm{V}}$ and $\bar{k}_{\mathrm{V}}$ are the vapour thermal diffusivity and conductivity, evaluated at the average vapour temperature, respectively and $\dot{Q}_{\mathrm{roof}}$ can be either a fixed value or it can be evaluated from an equation analogous to Eq. (5).

The initial and boundary conditions indicate that (i) the vapour is at thermal equilibrium with the liquid at the beginning of the evaporation, (ii) the vapour and liquid are in thermal equilibrium at their interface, and (iii) the roof can be subject to homogeneous and non-homogeneous Neumann or Robin boundary conditions. In Huerta & Vesovic model [43], the roof was assumed insulated ($\dot{Q}_{\mathrm{roof}} = 0$), whereas in

the present work, analytical solutions for Neumann and Robin boundary conditions are derived.

2.2. Analytical solutions for the evaporation of a pure cryogen in a cylindrical tank

The presented weathering model, Eqs. (1)-(8), simplifies considerably for the evaporation of a pure cryogen which, for a given operating pressure, takes place at the cryogen saturation temperature; thus, all the liquid thermophysical properties can be taken as constant. The Eq. (3), that describes the rate of decrease of liquid volume, reduces to

$$\frac{dV_{\mathrm{L}}}{dt} = -\frac{1}{\rho_{\mathrm{L}}}\left(\frac{\dot{Q}_{\mathrm{L,tot}}}{h_{\mathrm{V}}(T_{\mathrm{L}}) - h_{\mathrm{L}}(T_{\mathrm{L}})}\right). \tag{9}$$

In order to derive an analytical solution, we further assume that the temperature of the surrounding air remains constant and provided that the bottom of the tank is externally heated, the heat ingress through the bottom is also constant.

In the following subsections, we will first examine the equilibrium evaporation model [26] where it is assumed that the vapour and liquid phases are in equilibrium during the evaporation. This will be followed by derivation of the analytical solutions for the non-equilibrium evaporation model [43] where it is assumed that the ingress of heat will not only lead to the evaporation of the liquid, but also to heating the vapour above saturation temperature.

2.2.1 Analytical solutions for the equilibrium evaporation model

In the equilibrium model it is assumed that the vapour and liquid are in thermal equilibrium, $T_{\mathrm{L}} = T_{\mathrm{V}}$, and that all the heat entering the vapour contributes to evaporating the liquid, $\dot{Q}_{\mathrm{VL}} = \dot{Q}_{\mathrm{V}}$. Substituting the wall heat ingresses, Eq. (5), into Eq. (4), expresses the total liquid heat ingress as a linear function of the volume. Incorporating the resulting expression into Eq. (9) yields a first-order, linear, ordinary differential equation (ODE) with constant coefficients for the liquid volume,

$$\frac{dV_{\mathrm{L}}}{dt} = CV_{\mathrm{L}} + D\,, \tag{10}$$

where

$$C = -\frac{4d_{\mathrm{o}}}{d_{\mathrm{i}}^2}\frac{(T_{\mathrm{air}}-T_{\mathrm{L}})}{\rho_{\mathrm{L}}(h_{\mathrm{V}}-h_{\mathrm{L}})}(U_{\mathrm{L}} - U_{\mathrm{V}})\,, \tag{11}$$

and

$$\mathrm{D} = -\frac{1}{\rho_{\mathrm{L}}(h_{\mathrm{V}}-h_{\mathrm{L}})}\left(\frac{4d_{\mathrm{o}}}{d_{\mathrm{i}}^2}(T_{\mathrm{air}} - T_{\mathrm{L}})U_{\mathrm{V}}V_{\mathrm{T}} + \dot{Q}_{\mathrm{bot}}\right). \tag{12}$$

Considering the initial conditions, $V_{\mathrm{L}}(0) = V_{L0}$, the solution of Eq. (10) is given by

$$V_{\mathrm{L}} = \frac{D}{C}(\exp(Ct) - 1) + V_{\mathrm{L0}}\exp(Ct)\,, \qquad t \le \tau_{\mathrm{f}}, \tag{13}$$

where τ_{f} is defined as the time required for the complete evaporation of the liquid, obtained by setting the Eq. (13) to zero, and it is given by,

$$\tau_{\mathrm{f}} = \frac{1}{C}\ln\left(1 + V_{\mathrm{L0}}\frac{C}{D}\right)^{-1} = -\frac{1}{C}\ln\left(1 + V_{\mathrm{L0}}\frac{C}{D}\right)\,. \tag{14}$$

The solution for the evaporation rate, $\dot{B}_{\mathrm{L}}$, is obtained by simply multiplying Eq. (10) by the liquid density, while the BOG rate is given by,

$$\dot{B}(t) = (\bar{\rho}_{\mathrm{V}} - \rho_{\mathrm{L}})\,(CV_{\mathrm{L}}(t) + D)\,. \tag{15}$$

Note that for the equilibrium model, the vapour average density is constant and equal to the vapour density evaluated at the liquid temperature. If the heat flux through the liquid is higher than through the vapour, ($U_{\mathrm{L}} > U_{\mathrm{V}}$, $C < 0$) the liquid volume, $V_{\mathrm{L}}(t)$, and the BOG rate will exhibit an exponential decrease, see Eqs. (13) and (15). Otherwise, $V_{\mathrm{L}}\,(t)$ will be concave and the BOG rate will increase with time. The analytical solutions simplify further when the heat transfer coefficients for both phases are the same ($U_{\mathrm{L}} = U_{\mathrm{V}}$). In this case, the coefficient $C = 0$, and consequently, as $D < 0$, the liquid volume decreases linearly with time,

$$V_{\mathrm{L}}(t) = V_{\mathrm{L0}} + Dt\,, \tag{16}$$

while the BOG rate is constant and equal to $D(\bar{\rho}_{\mathrm{V}} - \rho_{\mathrm{L}})$, as can be seen from Eq. (15).

2.2.2 Analytical solutions for the non-equilibrium evaporation model

There is a strong experimental and industrial evidence [27, 32, 42, 45, 46] that the vapour above the cryogen is not at the same temperature as the liquid, but rather that it is superheated. In Huerta and Vesovic non-equilibrium weathering model [43] it is assumed that the heat entering the vapour will lead to increase in its temperature and that the superheated vapour will act as additional heat source transferring heat to the liquid by conduction at the rate $\dot{Q}_{\mathrm{VL}}$, see Eq. (6).

In order to render possible the analytical solutions for a non-equilibrium model, we first make a number of simplifying assumptions. Simulations using Huerta and Vesovic weathering model in large storage tanks have shown that the vapour temperature profile, when expressed in dimensionless form, reaches a pseudo steady-state shortly after the beginning of the evaporation [43]. The temperature profile is similar to the steady-state solution of the advection-diffusion equation. In other words, at this stage the temporal variation of the vapour temperature is entirely a result of an increase of the amount of vapour due to evaporation. Hence, we neglect the explicit dependence of vapour temperature on time ($\partial T_{\mathrm{V}}/\partial t = 0$) in Eq. (7) and assume that the vapour temperature is governed by the steady-state advection-diffusion equation for a given vapour volume. Furthermore, simulations [43] have also shown that the vapour to liquid heat ingress is small and nearly constant during evaporation. Thus, we assume that the advective vapour velocity, which was estimated in the weathering model from the evaporation rate, see the term multiplying the first spatial derivative of temperature in Eq. (7), is also constant, and it can be estimated from the initial evaporation rate $\dot{B}_{\mathrm{L0}}$, Eqs. (1) and (9),

$$\bar{v}_z \equiv \frac{4\dot{B}_{\mathrm{L0}}}{\bar{\rho}_{\mathrm{V}}\pi \mathrm{d}_{\mathrm{i}}^2} = \frac{4\dot{Q}_{\mathrm{L,tot}}}{\bar{\rho}_{\mathrm{V}}\pi d_{\mathrm{i}}^2 (h_{\mathrm{V}} - h_{\mathrm{L}})}. \tag{17}$$

Finally, we make the usual assumption that the variation of the vapour thermophysical properties is a weak linear function of the temperature, and that all vapour thermophysical properties are evaluated at the average vapour temperature. By making these assumptions we can transform the advection-diffusion equation, Eq. (7), into a second order, non-homogeneous, linear ODE with constant coefficients,

$$\bar{k}_{\mathrm{V}} \frac{d^2 T_{\mathrm{V}}}{dz^2} - H \frac{dT_{\mathrm{V}}}{dz} - S T_{\mathrm{V}} = -E \,, \tag{18}$$

where

$$H = \bar{\rho}_{\mathrm{V}} \bar{c}_{\mathrm{p,V}} \bar{v}_z, \quad S = \frac{4 U_{\mathrm{V}} d_{\mathrm{o}}}{d_{\mathrm{i}}^2}, \quad E = S T_{\mathrm{air}} \,, \tag{19}$$

subject to the boundary conditions,

$$T_{\mathrm{V}}|_{z=0} = T_{\mathrm{L}} \,, \tag{20}$$

$$\left.\frac{dT_{\mathrm{V}}}{dz}\right|_{z=l_{\mathrm{V}}} = \frac{\dot{Q}_{\mathrm{roof}}}{k_{\mathrm{V}}|_{z=l_{\mathrm{V}}} A_{\mathrm{roof}}} \,. \tag{21}$$

The discriminant of the characteristic equation associated with the homogeneous solution of Eq. (18), $\Delta = \sqrt{H^2 + 4\bar{k}_{\mathrm{V}} S}$, is always positive. Therefore, the vapour temperature profile is a linear combination of two exponential functions and the particular solution $T_{\mathrm{V}}(z) = T_{\mathrm{air}}$,

$$T_{\mathrm{V}}(z) = c_1 \exp(z\chi_-) + c_2 \exp(z\chi_+) + T_{\mathrm{air}} \,, \tag{22}$$

where

$$\chi_{\pm} = \frac{H \pm \sqrt{H^2 + 4\bar{k}_{\mathrm{V}} S}}{2\bar{k}_{\mathrm{V}}} \,. \tag{23}$$

The average vapour temperature, $\bar{T}_{\mathrm{V}} = \frac{1}{l_{\mathrm{V}}} \int_0^{l_{\mathrm{V}}} T_{\mathrm{V}}(z) dz$, can be obtained by directly integrating Eq. (22),

$$\bar{T}_{\mathrm{V}}(l_{\mathrm{V}}) = T_{\mathrm{air}} + \frac{1}{l_{\mathrm{V}}} \left(\frac{c_1}{\chi_-} \left(\exp\left(l_{\mathrm{V}} \chi_-\right) - 1 \right) + \frac{c_2}{\chi_+} \left(\exp\left(l_{\mathrm{V}} \chi_+\right) - 1 \right) \right), \tag{24}$$

where c_1 and c_2 are arbitrary constants that can be evaluated by ensuring that the solution satisfies the boundary conditions. The boundary condition at the vapour liquid interface is of Dirichlet type, while at the tank roof, there are two possibilities which depend on the value of $\dot{Q}_{\mathrm{roof}}$. We first consider a fixed heat ingress through the roof. In this case, the boundary conditions are of Dirichlet type at $z = 0$ and of Neumann type at $z = l_{\mathrm{V}}$. The constants c_1 and c_2 are given by,

$$c_1 = \frac{a_+(T_{\mathrm{L}} - T_{\mathrm{air}}) - \left.\frac{dT_{\mathrm{V}}}{dz}\right|_{z=l_{\mathrm{V}}}}{a_+ - a_-}, \quad c_2 = \frac{a_-(T_{\mathrm{air}} - T_{\mathrm{L}}) + \left.\frac{dT_{\mathrm{V}}}{dz}\right|_{z=l_{\mathrm{V}}}}{a_+ - a_-}, \tag{25}$$

where

$$a_\pm = \chi_\pm b_\pm , \tag{26}$$

$$b_\pm = \exp(l_{\mathrm{V}}\chi_\pm) , \tag{27}$$

$$\left.\frac{dT_{\mathrm{V}}}{dz}\right|_{z=l_{\mathrm{V}}} = \frac{\dot{Q}_{\mathrm{fixed}}}{k_{\mathrm{V}}|_{z=l_{\mathrm{V}}} A_{\mathrm{roof}}} , \tag{28}$$

In the second case we consider a variable heat ingress through the roof which depends on the roof temperature. In this case, the boundary conditions are of Dirichlet type at $z = 0$ and of Robin type at $z = l_{\mathrm{V}}$. The constants c_1 and $c_2$are given by,

$$c_1 = \frac{(T_{\mathrm{L}} - T_{\mathrm{air}})(a_+ + \gamma b_+)}{(a_+ + \gamma b_+) - (a_- + \gamma b_-)}, \quad c_2 = \frac{(T_{\mathrm{air}} - T_{\mathrm{L}})(a_- + \gamma b_-)}{(a_+ + \gamma b_+) - (a_- + \gamma b_-)}, \tag{29}$$

where

$$\gamma = \frac{U_{\mathrm{roof}}}{k_{\mathrm{V}}|_{z=l_{\mathrm{V}}}} . \tag{30}$$

We observe that the temporal variation of the vapour temperature is primarily governed by the height of the vapour phase, l_{V}, which increases during evaporation, due to the reduction in liquid volume. The analytical solutions for the vapour temperature profile enable us to calculate the vapour to liquid heat ingress, $\dot{Q}_{\mathrm{VL}}$,

$$\dot{Q}_{\mathrm{VL}} = \frac{\pi d_{\mathrm{i}}^2}{4} k_{\mathrm{V}}|_{z=0} (c_1\chi_- + c_2\chi_+) . \tag{31}$$

The vapour to liquid heat ingress, $\dot{Q}_{\mathrm{VL}}$, depends on the average thermophysical properties and the height of the vapour phase, see Eqs. (19, 23, and 24). These quantities change slowly during the evaporation. Consequently $\dot{Q}_{\mathrm{VL}}$ changes slowly with time and if we assume a constant value, the total liquid heat ingress becomes a linear function of liquid volume, as can be seen in Eqs. (4)-(5). Therefore, the rate of change of liquid volume is also linear in V_{L}, see Eq. (9), and the liquid volume is obtained from Eq. (13) by substituting the coefficients C and D by the non-equilibrium coefficients C^{neq}, D^{neq}, defined as,

$$C^{\mathrm{neq}} = -\frac{4d_{\mathrm{o}}}{d_{\mathrm{i}}^2}\frac{(T_{\mathrm{air}}-T_{\mathrm{L}})}{\rho_{\mathrm{L}}(h_{\mathrm{V}}-h_{\mathrm{L}})}U_{\mathrm{L}}\,, \tag{32}$$

and

$$D^{\mathrm{neq}} = -\frac{\dot{Q}_{\mathrm{bot}}+\dot{Q}_{\mathrm{VL}}}{\rho_{\mathrm{L}}(h_{\mathrm{V}}-h_{\mathrm{L}})}\,. \tag{33}$$

In a similar way, the time for complete evaporation and BOG rates for the non-equilibrium model are obtained by substituting the non-equilibrium coefficients in Eqs. (14) - (15), respectively.

We observe that for both equilibrium and non-equilibrium models, the reduction of the liquid volume, Eq. (13), and the BOG rates, Eq. (15), have the same form. Bearing in mind that $\rho_{\mathrm{V}} \ll \rho_L$ the non-equilibrium model will predict lower BOG rates and higher liquid volumes compared to the equilibrium model, as in the equilibrium model, $\dot{Q}_{\mathrm{VL}} = \dot{Q}_{\mathrm{V}}$, while in non-equilibrium model, $\dot{Q}_{\mathrm{VL}} < \dot{Q}_{\mathrm{V}}$. We observe further that under conditions of no heat transfer into or out of the vapour phase ($U_{\mathrm{V}} = \dot{Q}_{\mathrm{VL}} = 0$), the equilibrium constants C and D reduce to the non-equilibrium ones.

2.2.3 Implementation

The analytical solutions for the equilibrium case can be implemented directly using the thermophysical properties of both phases evaluated at the saturation temperature. For the non-equilibrium case, the situation is more complicated as the

analytical solutions for the vapour temperature, Eqs. (22-24, 26-30), and for the vapour to liquid heat transfer, Eq. (31), are functions of height of the vapour phase l_{V}. Hence, these two quantities can be only obtained sequentially, starting from the initial state where the height of the vapour phase is a known input. As the evaporation proceeds, the decrease in liquid volume will provide an appropriate value of l_{V}. Furthermore, the solution for both quantities requires an evaluation of the thermophysical properties $\bar{c}_{\mathrm{p}}$ and $\bar{k}_{\mathrm{V}}$, see Eqs. (18)-(19), and the advective velocity $\bar{v}_z$, see Eq. (17), at the average vapour temperature. To calculate T_{V} and $\dot{Q}_{\mathrm{VL}}$ at the given l_{V}, the first option is to assume that for the calculation of the vapour thermophysical properties the average vapour temperature is equal to the liquid boiling temperature, and that $\dot{Q}_{\mathrm{VL}}$ is negligible in the calculation of $\bar{v}_z$. This option is straightforward to implement, but it introduces an error which will increase with the duration of evaporation. The second option is to adopt an iterative approach. In the first iteration, the vapour temperature profile is obtained by evaluating the thermophysical properties at $\bar{T}_{\mathrm{V}} = T_{\mathrm{L}}$, and calculating $\bar{v}_z$ by assuming that $\dot{Q}_{\mathrm{VL}} = 0$. With the obtained temperature profile and $\dot{Q}_{\mathrm{VL}}$, $\bar{c}_{\mathrm{p}}$, $\bar{k}_{\mathrm{V}}$ and $\bar{v}_z$ are updated and so are the values of, H, c_1, c_2; that allows for a new vapour temperature profile and $\dot{Q}_{\mathrm{VL}}$ to be calculated. The iteration is repeated until the average vapour temperature converges to within acceptable limits. In this work the convergence criterium was 0.01K, which was achieved in less than 10 iterations.

The calculation of V_{L} and BOG is in principle straightforward as the Eqs (13,15) can be used directly if $\dot{Q}_{\mathrm{VL}}$ is assumed negligible in the total liquid heat ingress, see Eq. (4). However, a more accurate solution can be obtained if these two quantities are also calculated sequentially, using Eq. (31) to estimate the pseudo steady-state value of $\dot{Q}_{\mathrm{VL}}$ at each time step. The time step Δt is defined by partitioning the evaporation time in n_t intervals, $\Delta t = \tau_f / n_t$. We suggest using a time step between a week and a day, depending on the desired accuracy. To differentiate, in the rest of the paper, between the two calculation approaches we have named the former the direct route and the latter the sequential route. In order to help with the implementation, the numerical procedures used in this work are provided in a Python 3 Jupyter notebook as Supplementary Material. The analytical solutions were implemented in MATLAB® R2018b, and the

thermophysical properties of the cryogenic liquids were evaluated using the REFPROP 9.0 library [47].

3. Results

The analytical solutions were compared to the numerical results of Huerta and Vesovic weathering model [43] for large, medium sized and small tanks with different initial fillings, using methane and nitrogen as representatives of cryogenic liquids. No comparison with experimental data has been carried out in this work, as such validation has already been performed successfully for the numerical model [43]. The vapour properties were obtained at average vapour temperature by means of an iterative approach described in Section 2.2.3.

3.1 Evaporation of liquid methane in large storage tanks

The analytical solutions for the equilibrium and non-equilibrium model were validated against the numerical results obtained by running the LNG weathering model [43] for liquid methane. It was assumed that the cryogen was stored in the same 165,000 m^3 cylindrical storage tank (d_i = 76.4 m, d_o = 80.0 m) that was used for simulating weathering of LNG. For the purposes of simulations, the heat ingress through the bottom was assumed constant, $\dot{Q}_\mathrm{b} = 60$ kW, the roof was assumed insulated, $\dot{Q}_\mathrm{roof} = 0$, while the heat transfer coefficients were taken as $U_\mathrm{V} = U_\mathrm{L} = 0.037\ \mathrm{W\,m^{-2}K^{-1}}$. Simulations for two different initial liquid fillings (LF), high ($LF = 0.97$) and low ($LF = 0.3$), were run until the stored cryogen was completely depleted. A dimensionless time was defined as $\tau = t/\tau_\mathrm{evap}$, where τ_evap, the time taken for the cryogen to completely evaporate, was taken from the simulation results.

For the equilibrium model, the analytical solutions reproduced the numerical results exactly, to within 0.001%, for all the parameters studied (heat ingresses, liquid volume, evaporation rate, BOG rate and evaporation time). We next consider the analytical solutions for the non-equilibrium model. In Fig. 2 the vapour temperature profiles predicted by the analytical solutions are compared for high (Fig. 2a) and low (Fig. 2b) initial liquid fillings with the results obtained from the full numerical model. The profiles are plotted against the dimensionless length, $\xi \equiv z/l_V$, as ξ provides a useful scale for visualisation as it takes into account the increase in vapour height with time.

Temperature profiles for six different stages of the evaporation are depicted, from the beginning of the evaporation until the cryogen is completely depleted, $\tau = 1$. The analytical temperature profiles show an excellent agreement for the high liquid filling case (Fig 2a) during the whole process of evaporation. The absolute average percentage deviation (AAD) and maximum deviations (MD) between the analytical and numerical temperature profiles decreases from 0.5% and 1.2% at $\tau = 5.5 \times 10^{-5}$ to 0.2% and 0.3% at $\tau = 1$, respectively. In contrast, for the low liquid filling (Fig. 2b), the agreement is poor at the beginning of the evaporation (AAD = 12.0%; MD = 32.5% at $\tau = 3.25 \times 10^{-3}$) and improves considerably for $\tau \geq 6.5 \times 10^{-3}$ (AAD $<$ 0.2%; MD $<$ 0.3%), as illustrated in Figure 2b.

The failure of the analytical solution at the beginning of the evaporation is due to the failure of the steady-state assumption to capture the transient dynamic of the rapid vapour heating. During the transient period the temperature profile is governed by the full advection-diffusion equation, Eq. (7), rather than by the ODE Eq. (18), as assumed for the analytical solution. The large deviations observed for low liquid fillings are due to the presence of large vapour volumes which necessitate longer transition periods. The transient time increases approximately linearly with the decrease in the liquid filling, consistent with the scaling $\tau_{\text{trans}} \sim l_{\text{V}}/\bar{v}_z$ [43], and for tank specifications used in this example corresponds to $\tau_{\text{trans.,97\%}} \sim 1.1 \times 10^{-4}$ (~ 12 hours) and to $\tau_{\text{trans.,30\%}} \sim 6.5 \times 10^{-3}$ (~ 11.5 days) for high and low LF, respectively. For the purposes of this work we estimated that the steady-state ($\tau \geq \tau_{\text{trans}}$) is achieved when the average vapour temperature and density profiles in the vapour phase change at a rate slower than 1% per day.

It is worth nothing that the analytical temperature profile near the vapour-liquid interface, $0 \leq \xi \leq 0.1$, agrees exceptionally well with numerical results even for low LF at the initial stages of the evaporation, (AAD=0.9%; MD=1.9% for $\tau = 3.25 \times 10^{-3}$ and $LF = 0.3$). High accuracy of the vapour temperature profile near the interface is a desirable feature of the analytical solution as the spatial temperature gradient at the interface governs the vapour to liquid heat transfer rate, see Eq. (6). Equally importantly the analytical solutions give very good estimates of the BOG temperature of methane

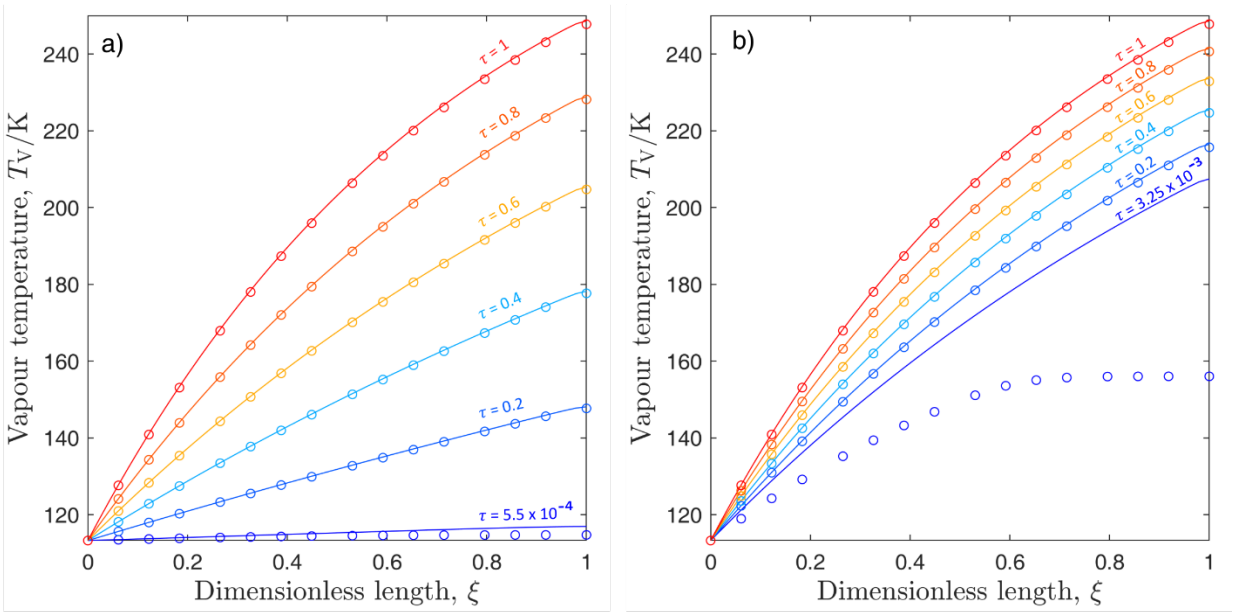

Figure 2: Vapour temperature profiles as a function of dimensionless length (ξ) and dimensionless time (τ) , for evaporation of liquid methane for: a) 97% initial liquid filling and b) 30% initial liquid filling. (----) analytical solutions and (o) numerical results from Huerta and Vesovic [43] weathering model.

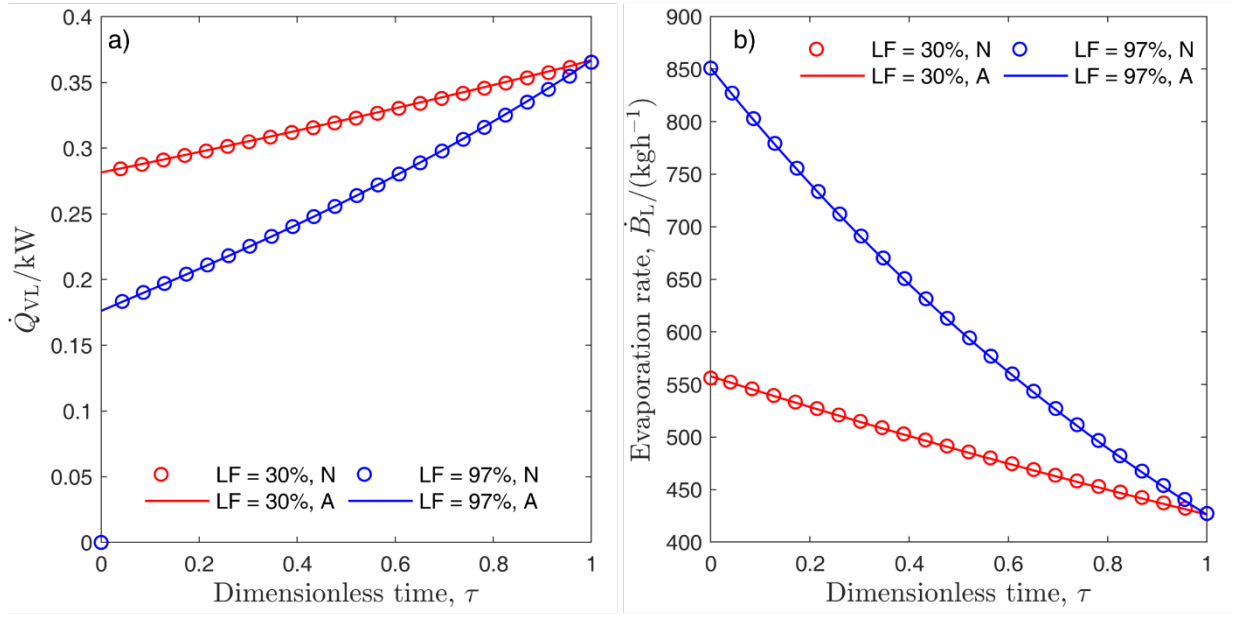

Figure 3: Vapour to liquid heat transfer rate, $\dot{Q}_{VL}$, (a) and evaporation rate, $\dot{B}_L$, (b) as a function of dimensionless time for the evaporation of liquid methane stored in a large tank at two different initial liquid fillings. (----) analytical solutions and (o) numerical results from Huerta and Vesovic [43] weathering model.

vapour, following the elapse of transitional period (AAD=0.1%, MD=0.2% for $\tau > \tau_{\text{trans}}$ and $LF = 0.3$).

In Fig.3 we analyse the performance of the analytical solutions in determining the vapour to liquid heat transfer rate (Fig. 3a) and the evaporation rate (Fig. 3b). The analytical solution predicts the vapour to liquid heat transfer with a high level of accuracy for both low (AAD = 0.2%) and high (AAD = 0.1%) liquid fillings after the initial transient period. The analytical model also predicts the evaporation rate exceptionally well, as illustrated in Fig 3b with the maximum deviation of 0.2% for both low and high LF. This result is not surprising, as total liquid heat ingress which drives the evaporation, Eq. (9), is dominated by heat transfer from the surrounding for which the proposed analytical solution is exact.

Figs. 4a illustrates the comparison of the BOG rates calculated from the analytical solution by direct route and by numerical simulation. We observe, see Figs 4b and 4c, that at the very beginning of the evaporation, the analytical solution underestimates the BOG rate for both high LF ($\tau < \tau_{\text{trans}}$, AAD = 1.0%; MD = 8.9%) and low LF ($\tau < \tau_{\text{trans}}$, AAD = 16.7%; MD = 55.2%). For $\tau > \tau_{\text{trans}}$ the agreement between the analytical and numerical results is excellent and low deviations in BOG rates are observed for both high LF (AAD = 0.4%, MD = 0.5%) and low LF (AAD = 0.3%, MD = 0.4%). Similarly, the agreement for liquid volumes was excellent for both high LF (AAD<0.1%, MD = 0.1%) and low LF (AAD=0.3%, MD=0.5%). Finally, we examine the evaporation times and report that the analytical model underestimates the numerical result by on average 0.5% irrespective of the initial liquid filling.

In order to test if the properties of the cryogen influence the observed deviations, we have repeated the validation using the same tank, but loaded with liquid nitrogen (LN_2). The deviations obtained were similar except for BOG rates during the transient period, see Figure 4d. The larger deviations for $\tau < \tau_{\text{trans}}$ are a result of a lower boiling point of nitrogen, which leads to a more rapid change of the vapour density with temperature. For $\tau > \tau_{\text{trans}}$, the agreement of BOG rates for both liquid fillings are similar to that observed for liquid methane (AAD = 0.5%, MD=0.6%).

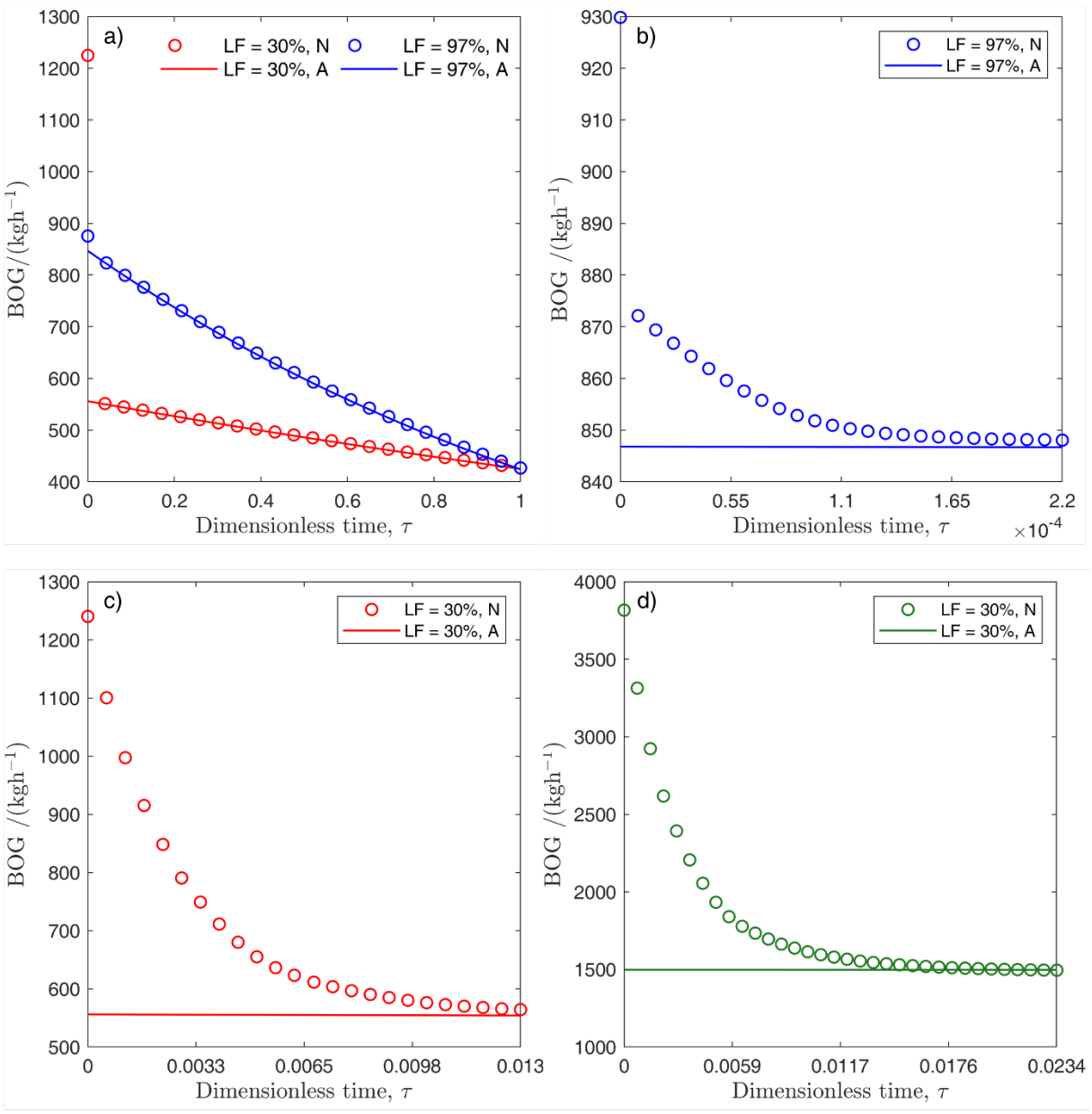

Figure 4: BOG rates during cryogen storage in a large tank as a function of dimensionless time for: a) evaporation of liquid methane at 97% LF; b) the initial transient period of evaporation of liquid methane at 97% LF; c) the initial transient period of evaporation of liquid methane at 30% LF; d) the initial transient period of evaporation of liquid nitrogen at 30% LF. (----) analytical solution and (o) numerical resultsp from Huerta and Vesovic [43] weathering model.

We have also repeated the calculation by estimating the thermophysical properties of the vapour at the cryogen saturation temperature, rather than average vapour temperature, thus avoiding the need for the iterative procedure described in

Section 2.2.3. The change in AAD (ΔAAD) between the two ways of calculating the analytical solution was negligible for evaporation rates and liquid volumes (ΔAAD<0.1%), and small for BOG rates (ΔAAD~0.4%) and for vapour and BOG temperatures (ΔAAD~1%). The increase of the maximum deviation, ΔMD, was negligible in all cases. This is to be expected as in the large tanks $\dot{Q}_{\mathrm{VL}}$ is small and evaporation rate, liquid volume and BOG rate are not governed by the thermophysical properties of vapour phase, see Eqs. (13, 14, 32, 33), in so far as the average vapour density is negligible compared with the liquid density, see Eq. (14). In contrast, the increase in the deviations observed for $\dot{Q}_{\mathrm{VL}}$ was moderate (ΔAAD~4%), with ΔMD = 6% for low LF and ΔMD = 18% for high LF.

3.2 Evaporation of liquid nitrogen stored in medium and small storage tanks

Not all the cryogens are stored in large storage tanks. As the size of the storage tank is reduced, the transient times decrease and at first sight one would expect the analytical solutions to be valid over an extended evaporation period. However, in smaller tanks the rate of vapour to liquid heat transfer, $\dot{Q}_{\mathrm{VL}}$, is proportionally greater and that could invalidate the assumption of small and constant $\dot{Q}_{\mathrm{VL}}$ used in deriving Eqs. (13, 32-33). Hence in this section, we examine the accuracy of the analytical solution for smaller tanks. In particular, we have tested the analytical solution for the case of liquid nitrogen storage in a medium-sized 80.4 m^3 cylindrical vessel ($d_{\mathrm{i}} = 2.85m\,, d_{\mathrm{o}} = 3.15\mathrm{m}, U_{\mathrm{L}} = U_{\mathrm{V}} = 0.011\ \mathrm{Wm^{-2}K^{-1}}$), as used in industry [15]. In this scenario, the tank is suspended from the floor and the bottom heat ingress is constant. At the tank roof, the heat transfer rate is dependent on the BOG temperature, see Eqs. (5) and (8), in contrast to the insulated roof assumption used previously for large tanks (see Sec. 3.1). Simulations were run for the two different fillings, namely high initial liquid filling (*LF*=0.97) and low initial liquid filling (*LF*=0.30), until the complete depletion of the stored liquid nitrogen.

As expected the transient periods for the medium-sized tank are an order of magnitude shorter than for the large tank, corresponding to $\tau_{\mathrm{trans.,97\%}} = 1 \times 10^{-4}$ (4

hours) and $\tau_{\mathrm{trans.,30\%}} = 8 \times 10^{-3}$ (5.1 days) for high and low initial liquid fillings, respectively. Figure 5 depicts analytical and numerical temperature profiles for the nitrogen vapour after the transient period ($\tau > \tau_{\mathrm{trans}}$). The temperature profiles show significantly higher curvature than the profiles for the large tank, see Fig. 2. As the Peclet numbers for both tanks are similar (in the medium sized tank Pe ranges from 0.95 to 8.7, whereas in the large tank Pe ranges from 0.98 to 14), one can conclude that the effect of conduction and advection is comparable. Hence, the higher curvature for medium-sized tank can be primarily attributed to increase of the contribution of the source term, *S*, with decreasing tank diameter, see Eqs. (18)-(19). Although the analytical temperature profiles showed a fair agreement with numerical results for both high LF (AAD = 1.1%, MD = 4.5%) and low LF (AAD = 0.8%, MD = 2.2%), the deviations are approximately five times higher than the deviations observed for the large tank (see Sec 3.1).

The increase in deviations, as the tank size decreases, can be attributed to the increase in magnitude of the vapour to liquid heat transfer rate, $\dot{Q}_{\mathrm{VL}}$. The average ratio of the vapour to liquid heat ingress to the total liquid heat ingress, $r_{\mathrm{q}} = \int_0^{\tau_{\mathrm{evap}}} \dot{Q}_{\mathrm{VL}} / \dot{Q}_{\mathrm{L,tot}}\, dt$, in the medium-sized tank is an order of magnitude higher than in the large tank; for the medium-sized tank, r_{q} = 3.3% for LF = 0.30 and r_{q} = 1.6% for LF = 0.97, whereas in the large tank, r_{q} = 0.33% for LF = 0.30 and r_{q} = 0.23% for LF = 0.97. Figure 6a, illustrates that not only is $\dot{Q}_{\mathrm{VL}}$ on average an order of magnitude higher, when going from a medium-sized to large storage tank, but that the rate of change of $\dot{Q}_{\mathrm{VL}}$, during evaporation, is approximately 3 to 8 times faster than for the large tank, see Fig. 3a. Thus, not corroborating the assumption of either small or constant $\dot{Q}_{\mathrm{VL}}$ made in deriving the analytical solution. Furthermore, the temperature profile is very sensitive to the estimation of the advective velocity. As $\dot{Q}_{\mathrm{VL}}$ increases eight times during the evaporation for high LF, compared with only three times for low LF, the observed deviations for temperature profiles are larger for high LF. Nevertheless, the vapour temperature profiles near the interface, are predicted for both LFs with deviations lower than 1%, which results in analytical solution, Eq. (31), predicting the vapour to liquid heat ingress

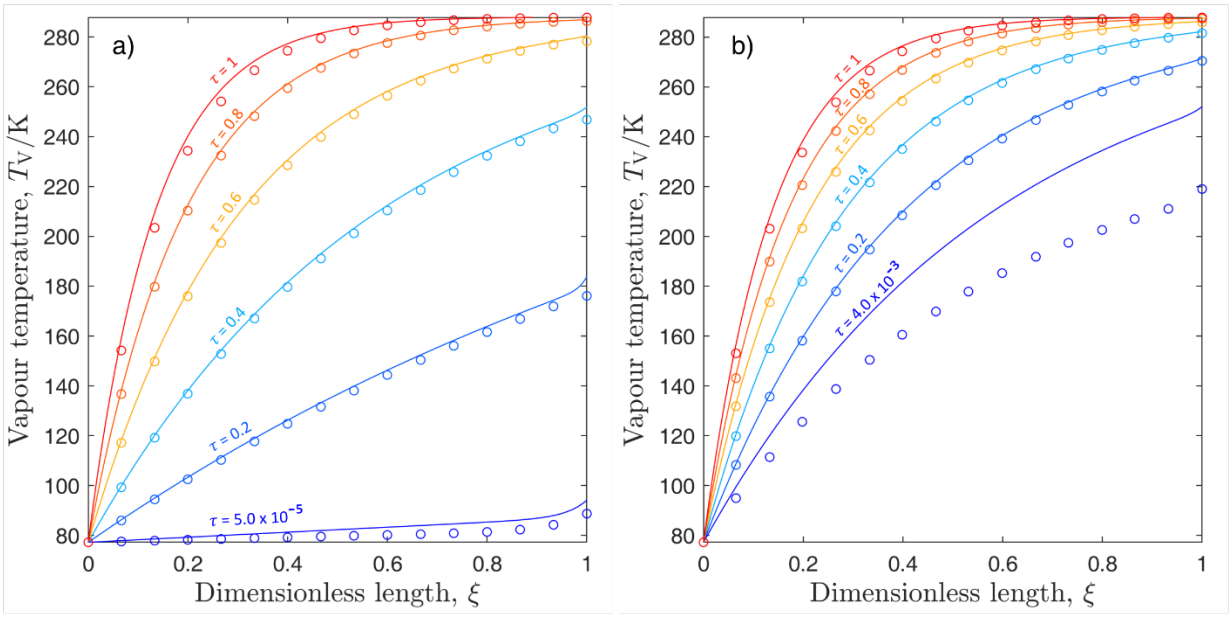

Figure 5: Vapour temperature profiles as a function of dimensionless length (ξ) and dimensionless time (τ), for the transient evaporation of liquid nitrogen in a medium-sized storage tank for: a) 97% initial liquid filling and b) 30% initial liquid filling. (----) analytical solutions and (o) numerical results from Huerta and Vesovic [43] weathering model.

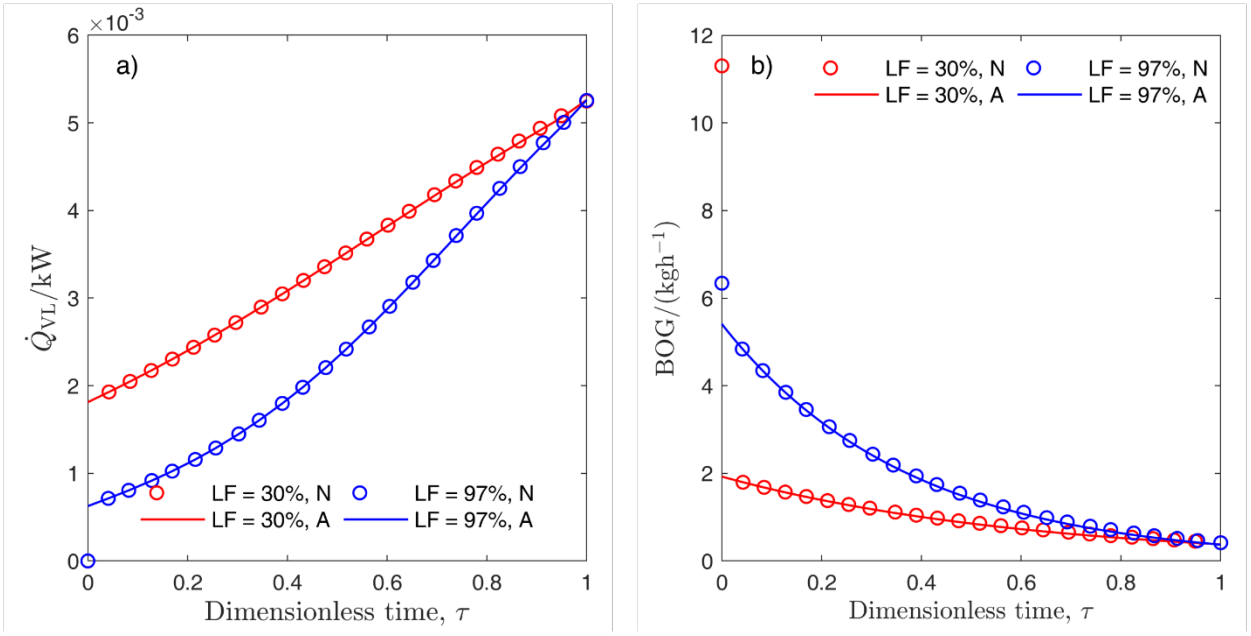

Figure 6: Vapour to liquid heat transfer rate (a) and BOG rates (b) during liquid nitrogen storage as a function of dimensionless time for the whole evaporation time for two different initial liquid fillings (LF). (----) analytical solution and (o) numerical results from Huerta and Vesovic [43] weathering model.

exceptionally well for both low LF (AAD =0.4%, MD =0.5%) and high LF (AAD = 0.1%, MD = 0.5%).

Analytical BOG rates, obtained by direct route, showed a good agreement with the numerical results, following the transient period, for both *LF* = 0.3 (AAD = 2.5%, MD = 3.9%) and *LF* = 0.97 (AAD =1.8 %, MD = 2.4%). Similarly, to temperature profile deviations, we observe that the BOG deviations are on average ten times larger than those for large storage tanks. However, if the BOG rates were calculated sequentially, by updating the value of $\dot{Q}_{\mathrm{VL}}$ at each step, as described in Section 2.2.3, the deviations are much smaller for both low LF (AAD = 0.1%, MD = 0.5%) and high LF (AAD =0.3%, MD = 1.1%) on par with the results for the large storage tank. The comparison between direct and sequential route of calculating the liquid volume and BOG temperature is given in Table 1. The results indicate that the sequential calculation presents a much improved estimate of all the quantities of interest to practising engineer.

Table 1

Deviations of the analytical solutions from the full results [43**]**, for the evaporation of liquid nitrogen in a medium sized tank using direct (D) and sequential (S) implementation

	LF=0.97				LF=0.30			
	AAD		MD		AAD		MD	
	D	S	D	S	D	S	D	S
$\boldsymbol{V}_{\mathbf{L}}$	0.9%	0.5%	3.0%	0.6%	1.5%	0.6%	4.7%	0.7%
BOG	1.2%	0.3%	2.0%	1.1%	2.0%	0.1%	3.4%	0.5%
$\boldsymbol{T}_{\mathrm{BOG}}$	1.2%	1.0%	2.4%	2.4%	0.2%	0.0%	0.4%	0.0%

To establish the range of applicability of the analytical solutions, simulations were also ran for a limiting case of liquid nitrogen stored in a small storage tank of 8 m^3 capacity ($d_{\mathrm{i}} = 1.604\ \mathrm{m}, d_{\mathrm{o}} = 1.630\ \mathrm{m}, U_{\mathrm{L}} = U_{\mathrm{V}} = 0.02\ \mathrm{W/m^2K}$, P=0.1 MPa, T=15 °C). Table 2 summarizes the deviations observed for the liquid volume, BOG rates and BOG temperature for both the direct and sequential calculations.

Table 2

Deviations of the analytical solutions, from the full results [43], for the evaporation of liquid nitrogen in a small tank using direct (D) and sequential (S) implementation

	LF=0.97				LF=0.30			
	AAD		MD		AAD		MD	
	D	S	D	S	D	S	D	S
$\boldsymbol{V}_{\mathrm{L}}$	1.3%	0.8%	4.3%	1.0%	1.7%	0.8%	5.4%	1.0%
BOG	2.0%	0.4%	3.1%	1.8%	2.6%	0.2%	4.3%	0.7%
$\boldsymbol{T}_{\mathrm{BOG}}$	3.0%	2.4%	4.5%	4.4%	0.8%	0.1%	1.0%	0.1%

Although the direct calculation resulted in larger deviations than previously observed for large and medium-sized tank, the sequential calculation produced a very good agreement, in spite of much larger contribution of $\dot{Q}_{\mathrm{VL}}$ ($r_q = 6.0\%$ for *LF* = 0.97, $r_q = 18.6\%$ for *LF* = 0.3) that questions the assumption made in deriving the analytical expressions that $\dot{Q}_{\mathrm{VL}}$ term is small and constant. The agreement in the vapour to liquid heat transfer rate was also good for both high LF (AAD = 0.4%, MD = 4.4%) and low LF (AAD = 1.4%, MD = 2.3%), as a consequence of good agreement in the temperature profiles near the interface.

Evaluating the vapour properties at the saturation temperature, rather than at the average vapour temperature, resulted in only a small increase in deviations for estimating BOG rates ($\Delta AAD_{small\ tank}$~0.4%), liquid volume ($\Delta AAD_{small\ tank}$~0.6%) and BOG temperature ($\Delta AAD_{small\ tank}$~1.5%). Although the deviations increase with a decrease in the size of the storage vessel, overall they were of similar magnitude as those observed for the large tanks and discussed in the previous section. Thus, rendering the need to perform an iterative temperature loop in order to obtain properties at the average vapour temperature unnecessary for estimating BOG rates, liquid

volume and BOG temperature. However, the calculation of the vapour temperature profiles and especially the vapour to liquid heat transfer rate using saturation temperature resulted in large deviations thus for these two quantities requiring a full iterative solution.

Conclusions

Analytical solutions for the isobaric evaporation of a liquid cryogen in a cylindrical tank have been presented for the liquid volume, BOG rate, vapour temperature and vapour to liquid heat transfer rate for both equilibrium and non-equilibrium weathering models. The solutions were verified against the numerical results of the Huerta & Vesovic weathering model [43]. For the equilibrium model, the solutions are exact, regardless of the tank size or cryogen, as the only assumptions made in the derivation are constant air temperature and constant heat ingress through the bottom of the tank. For the non-equilibrium model, the analytical solutions are valid for the whole duration of evaporation, except for a short transient period at the beginning of the evaporation. They provide accurate estimates of liquid volume, BOG rate and BOG temperature; the three quantities that are of particular interest to practising engineers. Although the accuracy decreases with the size of the storage tank, the maximum deviations did not exceed 1% for liquid volumes, 2% for BOG rates and 4.5% for BOG temperatures, for the range of different size tanks employed in this work. In order to achieve the aforementioned level of accuracy the calculation of liquid volume and BOG rate needs to be performed sequentially from the beginning of the evaporation with updating the vapour to liquid heat transfer at each time step. A direct evaluation, at a given time, of liquid volume and BOG rate would only lead to accurate results for the large storage tanks that are currently used to store LNG. The analytical solutions also provide accurate estimates of the vapour temperature profiles and the vapour to liquid heat transfer rate. For large storage tanks, the relevant vapour thermophysical properties can be estimated at the saturation temperature. As the size of the tank decreases the calculation needs to be performed at the average vapour temperature in order to maintain the desired accuracy. This requires an iterative approach.

One of the rationales in deriving the analytical solutions was to provide us with further insight into the evaporation process. We observe that the resulting analytical solutions for the vapour temperature clearly indicate that following the transient period, the temporal evolution of the profiles is primarily governed by the increase in the vapour height; the system reaches a pseudo steady-state with respect to heat ingress and the

increase in the vapour temperature is a result of a lower volume of liquid being present. We also observe that the contribution of the source term to the overall heat ingress increases with decreasing tank diameter. Thus, for smaller tanks, the evolution of the vapour temperature profiles, which exhibit large curvatures, is driven more by heat ingress from outside and less by conduction or advection, as is the case for large storage tanks. Finally, we observe that the analytical solution for the vapour to liquid heat transfer, $\dot{Q}_{\mathrm{VL}}$, is in a very good agreement with the numerical results. Even for the smallest tank, where the contribution of $\dot{Q}_{\mathrm{VL}}$ is large and increases with time, the maximum deviation is below 5%. This indicates that the analytical solution for $\dot{Q}_{\mathrm{VL}}$ can be used as a building block in more complex evaporation models.

Furthermore, by examining the analytical solutions we can conclude that the BOG rate is mainly governed by the evolution of the liquid volume, because the vapour density term is negligible in comparison to the liquid density. The variation in BOG rates will be greatest for small tanks with a poor insulation (small d_{i} and large U) as a consequence of increase in constant C. If the heat transfer through the bottom of the tank and vapour to liquid heat transfer are small, compared to the heat transfer through the walls, the constant D in the analytical solution will be small and the BOG rates will decrease exponentially through the evaporation, leading to longer evaporation times.

Acknowledgments

F. Huerta would like to acknowledge a postgraduate grant from the National Commission for Scientific and Technological Research (CONICYT) of Chile (CONICYT PFCHA/DOCTORADO BECAS CHILE/2017 – 72180177) that supported his work.

References

[1] Y. Yildiz, M. Nalbant, A review of cryogenic cooling in machining processes, Int. J. Mach. Tool. Manu., 48(9) (2008) 947-964.
[2] Y. Liu, K. Guo, A novel cryogenic power cycle for LNG cold energy recovery, Energy, 36(5) (2011) 2828-2833.
[3] R.W. Arnett, R.O. Voth, A computer program for the calculation of thermal stratification and self-pressurization in a liquid hydrogen tank, National Aeronautics and Space Administration, 1972.
[4] M. Voldsund, K. Jordal, R. Anantharaman, Hydrogen production with CO2 capture, Int. J. Hydrogen Energy, 41(9) (2016) 4969-4992.
[5] T. Zhang, L.J. Chen, X.L. Zhang, S.W. Mei, X.D. Xue, Y. Zhou, Thermodynamic analysis of a novel hybrid liquid air energy storage system based on the utilization of LNG cold energy, Energy, 155 (2018) 641-650.
[6] M. Aneke, M. Wang, Energy storage technologies and real life applications – A state of the art review, Appl. Energy, 179 (2016) 350-377.
[7] B. Sreenivasulu, D.V. Gayatri, I. Sreedhar, K.V. Raghavan, A journey into the process and engineering aspects of carbon capture technologies, Renew. Sust. Energ. Rev., 41 (2015) 1324-1350.
[8] Y.N. Wang, J.M. Pfotenhauer, X.Q. Zhi, L.M. Qiu, J.F. Li, Transient model of carbon dioxide desublimation from nitrogen-carbon dioxide gas mixture, Int. J. Heat Mass Transfer, 127 (2018) 339-347.
[9] C. Song, Q. Liu, S. Deng, H. Li, Y. Kitamura, Cryogenic-based CO2 capture technologies: State-of-the-art developments and current challenges, Renew. Sust. Energ. Rev, 101 (2019) 265-278.
[10] GIIGNL, Rollover in LNG Storage Tanks, 2015.
[11] S. Gursu, S.A. Sherif, T.N. Veziroglu, J.W. Sheffield, Analysis and optimization of thermal stratification and self-pressurization effects in liquid-hydrogen storage-systems - Part 1: Model development., J Energ. Resour. Asme, 115(3) (1993) 221-227.
[12] Z. Liu, Y. Li, G. Zhou, Study on thermal stratification in liquid hydrogen tank under different gravity levels, Int. J. Hydrogen Energy, 43(19) (2018) 9369-9378.
[13] S.M. Aceves, G.D. Berry, G.D. Rambach, Insulated pressure vessels for hydrogen storage on vehicles, Int. J. Hydrogen Energy, 23(7) (1998) 583-591.

[14] A. Hofmann, Theory to boil-off gas cooled shields for cryogenic storage vessels, Cryogenics, 44(3) (2004) 159-165.
[15] Cryogenic Standard Tanks LITS 2, Linde AG, Engineering Division, Tacherting, Germany, 2019.
[16] R. Dutta, P. Ghosh, K. Chowdhury, Process configuration of Liquid-nitrogen Energy Storage System (LESS) for maximum turnaround efficiency, Cryogenics, 88 (2017) 132-142.
[17] S.W. Churchill, Heat leakage and wall temperature profiles for above ground low-temperature storage tanks, Chem. Eng. Prog., 58(11) (1962) 55-60.
[18] J. Joseph, G. Agrawal, D.K. Agarwal, J.C. Pisharady, S.S. Kumar, Effect of insulation thickness on pressure evolution and thermal stratification in a cryogenic tank, Appl. Therm. Eng., 111 (2017) 1629-1639.
[19] G. Agrawal, J. Joseph, D. Agarwal, J.C. Pisharady, S.S. Kumar, Iop, Mathematical Modelling of Thermal Stratification in a Cryogenic Propellant Tank, in: 26th International Cryogenic Engineering Conference & International Cryogenic Materials Conference 2016, 2017.
[20] D.T. Neill, H.T. Hashemi, C.M. Sliepcevich, Boil-off rates and wall temperatures in above ground LNG storage tanks, in: Chem. Eng. Prog. Symp., American Institute of Chemical Engineers., 1968, pp. 111-119.
[21] J.M. Shah, J.J. Aarts, Effect of weathering of LNG in storage tanks, in: Adv. Cryog. Eng., Springer US, Boston, 1995, pp. 253-260.
[22] M. Miana, R. Del Hoyo, V. Rodrigálvarez, J.R. Valdés, R. Llorens, Calculation models for prediction of Liquefied Natural Gas (LNG) ageing during ship transportation, Appl. Energy, 87(5) (2010) 1687-1700.
[23] Q.S. Chen, J. Wegrzyn, V. Prasad, Analysis of temperature and pressure changes in liquefied natural gas (LNG) cryogenic tanks, Cryogenics, 44(10) (2004) 701-709.
[24] L.A. Pellegrini, S. Moioli, F. Brignoli, C. Bellini, LNG technology: the weathering in above-ground storage tanks, Ind. Eng. Chem. Res., 53(10) (2014) 3931-3937.
[25] C. Migliore, A. Salehi, V. Vesovic, A non-equilibrium approach to modelling the weathering of stored Liquefied Natural Gas (LNG), Energy, 124 (2017) 684-692.
[26] C. Migliore, C. Tubilleja, V. Vesovic, Weathering prediction model for stored liquefied natural gas (LNG), J. Nat. Gas. Sci. Eng., 26 (2015) 570-580.
[27] M. Seo, S. Jeong, Analysis of self-pressurization phenomenon of cryogenic fluid storage tank with thermal diffusion model, Cryogenics, 50(9) (2010) 549-555.
[28] S. Roh, G. Son, G. Song, J. Bae, Numerical study of transient natural convection in a pressurized LNG storage tank, Appl. Therm. Eng., 52(1) (2013) 209-220.

[29] S. Roh, G. Son, Numerical study of natural convection in a liquefied natural gas tank, J. Mech. Sci. Technol., 26(10) (2012) 3133-3140.
[30] A. Saleem, S. Farooq, I.A. Karimi, R. Banerjee, A CFD simulation study of boiling mechanism and BOG generation in a full-scale LNG storage tank, Comput. Chem. Eng., 115 (2018) 112-120.
[31] C.H. Panzarella, M. Kassemi, On the validity of purely thermodynamic descriptions of two-phase cryogenic fluid storage, J. Fluid Mech., 484 (2003) 41-68.
[32] R.N. Krikkis, A thermodynamic and heat transfer model for LNG ageing during ship transportation. Towards an efficient boil-off gas management, Cryogenics, 92 (2018) 76-83.
[33] M. Kassemi, O. Kartuzova, S. Hylton, Validation of two-phase CFD models for propellant tank self-pressurization: Crossing fluid types, scales, and gravity levels, Cryogenics, 89 (2018) 1-15.
[34] K.J. Kountz, Weathering of LNG in on-board storage tanks, Institute of Gas Technology, Chicago, 1999.
[35] A. Aspelund, G. Gjøvåg, P. Nekså, K. Kolsaker, LNG—Chain, a calculation tool for natural gas quality in small scale LNG distribution chains, in: ICEC-21 International Cryogenic Engineering Conference 2007.
[36] A. Aspelund, T. Gundersen, J. Myklebust, M.P. Nowak, A. Tomasgard, An optimization-simulation model for a simple LNG process, Comput. Chem. Eng., 34(10) (2010) 1606-1617.
[37] G.G. Dimopoulos, C.A. Frangopoulos, A dynamic model for liquefied natural gas evaporation during marine transportation, Int. J. Thermodyn., 11(3) (2008) 123-131.
[38] E. Adom, Z.I. Sheikh, J. Xianda, Modelling of boil off gas in LNG tanks: a case study, IJET, 2(4) (2010) 292-296.
[39] S. Barsi, M. Kassemi, Numerical and experimental comparisons of the self-pressurization behavior of an LH2 tank in normal gravity, Cryogenics, 48(3) (2008) 122-129.
[40] C.H. Panzarella, M. Kassemi, Self-pressurization of large spherical cryogenic tanks in space, Journal of Spacecraft and Rockets, 42(2) (2005) 299-308.
[41] Y. Qu, I. Noba, X. Xu, R. Privat, J.-N. Jaubert, A thermal and thermodynamic code for the computation of Boil-Off Gas – Industrial applications of LNG carrier, Cryogenics, 99 (2019) 105-113.
[42] S. Effendy, M.S. Khan, S. Farooq, I.A. Karimi, Dynamic modelling and optimization of an LNG storage tank in a regasification terminal with semi-analytical solutions for N2-free LNG, Comput. Chem. Eng., 99 (2017) 40-50.

[43] F. Huerta, V. Vesovic, A realistic vapour phase heat transfer model for the weathering of LNG stored in large tanks, Energy, 174 (2019) 280-291.
[44] A. Sharafian, O.E. Herrera, W. Mérida, Performance analysis of liquefied natural gas storage tanks in refueling stations, J. Nat. Gas. Sci. Eng., 36 (2016) 496-509.
[45] M. Kang, J. Kim, H. You, D. Chang, Experimental investigation of thermal stratification in cryogenic tanks, Exp. Therm. Fluid Sci., 96 (2018) 371-382.
[46] Y. Lin, C. Ye, Y.Y. Yu, S.W. Bi, An approach to estimating the boil-off rate of LNG in type C independent tank for floating storage and regasification unit under different filling ratio, Appl. Therm. Eng., 135 (2018) 463-471.
[47] E. W. Lemmon, M. L. Huber, M.O. McLinden, NIST Standard Reference Database 23: Reference Fluid Thermodynamic and Transport Properties-REFPROP, Version 9.1, National Institute of Standards and Technology, in, 2013.